Astronomy Letters, Vol. 33, No. 6, 2007, pp. 368-384. Translated from Pis'ma v Astronomicheskii Zhurnal, Vol. 33, No. 6, 2007, pp. 417-434.

4U 0115+63 from RXTE and INTEGRAL Data: Pulse Profile and Cyclotron Line Energy

S. S. Tsygankov[1,2]*, A. A. Lutovinov[1,2], E. M. Churazov[2,1] and R. A. Sunyaev[2,1]

[1] *Space Research Institute, Profsoyuznaya str. 84/32, Moscow 117997, Russia*
[2] *MPI for Astrophysik, Karl-Schwarzschild str. 1, Garching, 85741, Germany*

We analyze the observations of the transient X-ray pulsar 4U 0115+63 with the RXTE and INTEGRAL observatories in a wide X-ray (3–100 keV) energy band during its intense outbursts in 1999 and 2004. The energy of the fundamental harmonic of the cyclotron resonance absorption line near the maximum of the X-ray flux from the source (luminosity range 5×10^{37} – 2×10^{38} erg s^{-1}) is $\sim$ 11 keV. When the pulsar luminosity falls below $\sim 5 \times 10^{37}$ erg s^{-1}, the energy of the fundamental harmonic is displaced sharply toward the high energies, up to $\sim$ 16 keV. Under the assumption of a dipole magnetic field configuration, this change in cyclotron harmonic energy corresponds to a decrease in the height of the emitting region by $\sim$ 2 km, while other spectral parameters, in particular, the cutoff energy, remain essentially constant. At a luminosity $\sim 7 \times 10^{37}$ erg s^{-1} , four almost equidistant cyclotron line harmonics are clearly seen in the spectrum. This suggests that either the region where the emission originates is compact or the emergent spectrum from different (in height) segments of the accretion column is uniform. We have found significant pulse profile variations with energy, luminosity, and time. In particular, we show that the profile variations from pulse to pulse are not reduced to a simple modulation of the accretion rate specified by external conditions.

Key words: pulsars, neutron stars, X-ray sources.

* E-mail: st@hea.iki.rssi.ru

INTRODUCTION

The X-ray source 4U 0115+63 was discovered by the UHURU observatory more than 30 years ago (Giacconi et al. 1972; Forman et al. 1978). During the SAS-3 observations in 1978, Rappaport et al. (1978) determined the binary's main parameters based on the known pulsation period of $\sim$ 3.6 s (Cominsky et al. 1978): orbital period $\sim$ 24.3 days, orbital eccentricity 0.34, and projected semimajor axis of the relativistic object $a_x \sin i \sim 140$ light seconds (see also Tamura et al. (1992) and Lutovinov et al. (1994) for an improvement of the parameters). The optical observations of the star V635 Cas (Hutchings and Crampton 1981; Kholopov et al. 1981), the normal companion of the X-ray source 4U 0115+63, performed by Negueruela and Okazaki (2001) allowed the star's spectral type to be improved, B0.2Ve, and the binary's distance to be estimated, 7–8 kpc.

In addition to its transient behavior (which ensures a wide dynamic range of the object's observed luminosities), the X-ray pulsar 4U 0115+63 is unique in its spectral characteristics. The cyclotron resonance absorption line was first detected in its spectrum almost 30 years ago. At present, it is the only object in the spectrum of which five cyclotron line harmonics were detected. The properties of the cyclotron feature in the source under consideration were studied in detail using data from many observatories (Wheaton et al. 1979; White et al. 1983; Mihara et al. 1998, 2004; Heindl et al. 1999; Santangelo et al. 1999; Lutovinov et al. 2000). It was shown that the source spectrum is subject to significant variations on a time scale shorter than the spin period of the neutron star and that different cyclotron frequency harmonics behave differently depending on the pulse phase; in particular, the third harmonic is present only on the descent of the second (smaller) peak of the pulse profile (Heindl et al. 1999). Mihara et al. (1998) found that only one cyclotron absorption harmonic at $\sim$ 16 keV was detected in the source spectrum during its observations in 1991 instead of the two lines at $\sim$ 12 and $\sim$ 22 keV observed in 1990. Using the RXTE data obtained during another intense outburst in MarchApril 1999, Nakajima et al. (2006) confirmed that the cyclotron line position in the source spectrum depends on the pulsar luminosity, while the single line at $\sim$ 16 keV is most likely the "upward"-displaced fundamental harmonic.

Despite many observations and studies of the X-ray pulsar 4U 0115+63, a number of poorly studied questions related to the variations in the source pulse profile and its spectral characteristics with source intensity and energy band still remain.

In this paper, we perform a timing analysis of the pulsar emission on the scale of the pulsation period and investigate its spectral properties as a function of the intrinsic luminosity using the RXTE and INTEGRAL data obtained during the 2004 outburst and RXTE data for the previous 1999 outburst.

OBSERVATIONS AND DATA ANALYSIS

In this paper, we use the observations of the X-ray pulsar 4U 0115+63 during its intense outbursts in MarchApril 1999 and SeptemberOctober 2004 with the instruments of the RXTE

orbital astrophysical observatory (Bradt et al. 1993) – the PCA and HEXTE spectrometers (observations 40051-05-XX-XX, 40070-01-XX-00, 40411-01-XX-00, 90014-02-XX-XX, and 90089-01-XX-XX) operating in the $3-20$ and $15-250$ keV energy bands, respectively. The PCA spectrometer is a system of five proportional xenon/propane counters with an effective area of $\sim$6400 cm^2 at 6–7 keV and an energy resolution of $\sim$18%. The HEXTE spectrometers is a system of two independent packages of four NaI(Tl)/CsI(Na) phoswich detectors swinging with an interval of 16 s for the observation of background areas at a distance of 1.5° from the source. At each specific time, the source can be observed only by one of the two detector packages; thus, the effective area of the HEXTE detectors is $\sim$700 cm^2 . The standard FTOOLS/LHEASOFT 5.3 software package was used to process the RXTE data.

To study in detail the properties of the hard (>20 keV) X-ray emission from the pulsar, we used the data from the IBIS telescope (ISGRI detector; Lebrun et al. 2003) of the INTEGRAL observatory (Winkler et al. 2003) obtained during its outburst that began late in August 2004 (Lutovinov et al. 2004). We processed the IBIS data for our timing analysis using the software developed and maintained at the National Astrophysical Institute in Palermo, Italy (http://www.pa.iasf.cnr.it/$\tilde{}$ferrigno/INTEGRALsoftware.html); a description of the data processing technique can be found in Mineo et al. (2006). For our spectral analysis, we used the software and methods developed at the Space Research Institute of the Russian Academy of Sciences (Moscow, Russia) and described in Revnivtsev et al. (2004). Analysis of a large set of calibration observations for the Crab Nebula showed that the uncertainties in the derived source energy spectra related to the evolution of the detector background and its characteristics do not exceed $\sim 3\%$. The latter was added as a systematic uncertainty during our spectral analysis with the XSPEC software package. For our spectral analysis at energies below 20 keV, we used JEM-X data (Lund et al. 2003), which were processed with the standard OSA 5.1 package provided by the INTEGRAL Science Data Center (http://isdc.unige.ch).

Tables 1 and 2 list the RXTE and INTEGRAL observations of the X-ray pulsar 4U 0115+63 in 1999 and 2004. Column 1 gives the observation date and number; columns 2 and 3 provide the flux from the source and its bolometric luminosity (calculated for an assumed distance to the source of 7 kpc) in the range of main energy release $3-100$ keV, respectively. The typical RXTE exposures times lie within the range from ~ 0.3 to ~ 4 ks; the INTEGRAL exposure time for the source is ~ 200 ks. All of the measurement errors given here correspond to 1σ.

THE PULSE PROFILE

The Average Pulse Profile, its Evolution with Luminosity and Energy

We analyzed the properties of the pulse profile using the data obtained during the 1999 outburst, since it had a wider luminosity range and was observed with the RXTE instruments from an earlier phase. The results of our analysis of the more recent observations in 2004 showed no significant differences from those obtained for the 1999 outburst. Assuming the distance to the binary to be 7 kpc, the range of observed luminosities for the source during its outburst was $\sim$ (1–15) $\times 10^{37}$ erg s^{-1} . Due to such a high intensity of the pulsar emission, we were able not only to trace the dependence of the pulse profile shape on the object's intrinsic luminosity in various energy bands with a good statistical significance, but also to investigate its variability on the scale of the pulsation period.

Figure 1 shows the background-corrected phase light curves of the pulsar 4U 0115+63 at various source luminosities in various energy bands obtained from RXTE data. In the figure, the columns are arranged from the outburst onset from left to right and correspond to luminosities $\sim 7.3 \times 10^{37}$, $\sim 14.6 \times 10^{37}$, $\sim 6.6 \times 10^{37}$ and $\sim 1.5 \times 10^{37}$ erg s^{-1}. The first and third columns reflect the evolution of the pulse profile with energy for the rise and decay of the outburst, respectively. We see that at the same intensity of the pulsar emission, the pulse profiles are almost identical irrespective of the outburst phase.

It is interesting to trace the evolution of the pulse profile shape with energy: in soft (< 20 keV) energy channels, the profile is double-peaked with a tendency for the second peak to disappear as the pulsar luminosity decreases; as the energy increases, the second peak also disappears and the profile becomes virtually single-peaked above ~ 20 keV, with the width of the first peak being ~ 0.5 of the phase, but the width of the first peak at about 30 keV increases and reaches ~ 0.75 of the phase, partially covering the region of the first peak. A distinctive feature of the average pulse profile for the source under study is the presence of several peculiarities in its shape–additional small peaks (e.g., at phases 0.14 and 0.92 in the observations with a luminosity $< 7 \times 10^{37}$ erg s^{-1}) and an asymmetry of the second (with a lower intensity) peak.

To qualitatively explain the observed behavior of the pulse profile (the decrease in the intensity of the second peak with decreasing luminosity and increasing energy), we can suggest a simple, purely geometrical picture that is capable of describing the main observed trends in the pulse profile in general terms: the rotation axis of the neutron star is inclined with respect to the axis of its magnetic field in such a way that the accretion column at one of the poles is seen over its entire (or almost entire) height when the pole falls on the observer's line of sight; only the upper part emitting softer photons is seen in the second column, while the emission region of hard photons is screened by the neutron-star surface (hence the observed decrease in the intensity of the second peak with increasing energy); as the accretion rate and, accordingly, the source luminosity decrease, the column height decreases, the intensity of the second peak falls, and we will cease to see it altogether at some time.

Table 1. RXTE observations of the pulsar 4U 0115+63 in 1999

Date, MJD (pointing)	Flux[a], $\times 10^{-9}$ erg s^{-1} cm^{-2}	Luminosity[b], 10^{37} erg s^{-1}
51240.15 (40411-01-01-00)	12.2 ± 1.1	7.2 ± 0.6
51241.56 (40411-01-02-00)	12.3 ± 1.0	7.3 ± 0.6
51242.87 (40411-01-03-00)	16.5 ± 0.9	9.7 ± 0.5
51243.87 (40411-01-04-00)	19.1 ± 1.2	11.2 ± 0.7
51244.31 (40070-01-01-00)	20.2 ± 0.1	11.9 ± 0.1
51244.87 (40411-01-05-00)	20.1 ± 1.3	11.8 ± 0.8
51246.27 (40411-01-06-00)	22.1 ± 1.7	13.0 ± 1.0
51246.83 (40411-01-07-00)	26.4 ± 2.0	15.5 ± 1.1
51247.76 (40411-01-08-00)	21.4 ± 1.3	12.6 ± 0.8
51248.38 (40411-01-09-00)	21.9 ± 1.4	12.9 ± 0.8
51248.94 (40070-01-02-00)	24.4 ± 1.1	14.4 ± 0.6
51249.16 (40070-01-03-00)	24.9 ± 0.3	14.6 ± 0.2
51249.76 (40411-01-10-00)	22.5 ± 1.4	13.2 ± 0.8
51250.80 (40411-01-11-00)	24.6 ± 1.3	14.5 ± 0.8
51251.28 (40411-01-12-00)	23.5 ± 1.4	13.8 ± 0.8
51252.34 (40411-01-13-00)	20.8 ± 1.5	12.3 ± 0.9
51253.40 (40411-01-14-00)	21.0 ± 1.1	12.3 ± 0.6
51254.61 (40411-01-15-00)	23.7 ± 1.4	13.9 ± 0.8
51255.33 (40411-01-16-00)	23.2 ± 1.5	13.6 ± 0.9
51256.22 (40051-05-01-00)	21.0 ± 0.8	12.3 ± 0.4
51256.54 (40411-01-17-00)	19.0 ± 0.8	11.2 ± 0.5
51257.16 (40411-01-18-00)	18.8 ± 1.2	11.1 ± 0.7
51258.31 (40051-05-02-00)	20.9 ± 0.9	12.3 ± 0.5
51258.55 (40411-01-19-00)	19.8 ± 0.7	11.6 ± 0.4
51259.20 (40411-01-20-00)	16.5 ± 0.8	9.7 ± 0.4
51260.29 (40051-05-03-00)	18.6 ± 1.0	10.9 ± 0.6
51260.42 (40411-01-21-00)	18.7 ± 2.0	11.0 ± 1.1
51261.54 (40411-01-22-00)	17.0 ± 1.1	10.0 ± 0.7
51262.23 (40051-05-04-00)	13.7 ± 0.4	8.1 ± 0.2
51263.25 (40411-01-23-00)	12.6 ± 1.2	7.4 ± 0.7
51264.39 (40051-05-05-00)	13.6 ± 0.7	8.0 ± 0.4
51265.19 (40070-01-04-00)	12.8 ± 0.1	7.5 ± 0.1
51266.07 (40051-05-06-00)	11.6 ± 0.3	6.8 ± 0.2
51266.32 (40070-01-05-00)	11.3 ± 0.1	6.6 ± 0.1
51268.22 (40051-05-07-00)	9.4 ± 0.5	5.5 ± 0.3
51269.16 (40051-05-15-02)	8.8 ± 0.3	5.2 ± 0.2
51270.22 (40051-05-08-00)	8.3 ± 0.1	4.9 ± 0.1
51271.11 (40051-05-15-01)	8.1 ± 0.7	4.7 ± 0.4
51272.21 (40051-05-09-00)	7.0 ± 0.1	4.1 ± 0.1
51273.47 (40051-05-15-00)	6.0 ± 1.0	3.5 ± 0.6
51274.14 (40051-05-10-00)	5.9 ± 0.1	3.5 ± 0.1
51276.09 (40051-05-11-00)	5.0 ± 0.3	2.9 ± 0.2
51278.21 (40051-05-12-00)	3.9 ± 0.1	2.3 ± 0.1
51280.14 (40051-05-13-00)	2.5 ± 0.2	1.5 ± 0.1
51282.09 (40051-05-14-00)	2.0 ± 0.1	1.2 ± 0.1
51284.92 (40411-01-24-00)	3.4 ± 0.2	2.0 ± 0.1
51286.92 (40411-01-25-00)	2.3 ± 0.2	1.4 ± 0.1
51288.06 (40411-01-26-00)	0.2 ± 0.3	0.1 ± 0.1

[a] In the 3100 keV energy band.

[b] In the 3100 keV energy band for an assumed source distance of $d = 7$ kpc.

Table 2. RXTE and INTEGRAL observations of the pulsar 4U 0115+63 in 2004

Date, MJD (pointing)	Flux[a], $\times 10^{-9}$ erg s^{-1} cm^{-2}	Luminosity[b], 10^{37} erg s^{-1}
From RXTE (PCA and HEXTE) data		
53260.18 (90089-01-03-01)	18.3 ± 2.4	10.8 ± 1.4
53262.20 (90089-01-03-00)	22.8 ± 2.4	13.4 ± 1.4
53265.08 (90089-01-04-06)	18.7 ± 0.6	11.0 ± 0.4
53267.24 (90089-01-04-04)	16.8 ± 0.5	9.9 ± 0.3
53269.13 (90089-01-04-02)	17.2 ± 0.4	10.1 ± 0.2
53270.51 (90089-01-04-00)	16.2 ± 0.6	9.5 ± 0.4
53271.97 (90089-01-04-03)	14.7 ± 0.1	8.6 ± 0.1
53272.82 (90089-01-05-00)	13.9 ± 0.3	8.2 ± 0.2
53272.96 (90089-01-05-05)	13.8 ± 0.4	8.1 ± 0.2
53274.85 (90089-01-05-01)	12.6 ± 1.4	7.4 ± 0.8
53275.69 (90089-01-05-02)	11.9 ± 0.6	7.0 ± 0.4
53276.75 (90089-01-05-03)	11.0 ± 0.2	6.5 ± 0.1
53278.65 (90089-01-05-04)	9.6 ± 0.4	5.6 ± 0.2
53280.73 (90089-01-06-00)	8.0 ± 1.0	4.7 ± 0.6
53282.65 (90014-02-01-00)	6.8 ± 0.1	4.0 ± 0.1
53284.62 (90014-02-01-02)	5.0 ± 0.1	2.9 ± 0.1
53285.99 (90014-02-01-01)	3.8 ± 0.4	2.2 ± 0.2
53287.83 (90014-02-02-00)	3.2 ± 0.4	1.9 ± 0.2
53289.54 (90014-02-02-01)	2.5 ± 0.3	1.5 ± 0.2
53290.65 (90014-02-02-02)	1.9 ± 0.1	1.1 ± 0.1
53291.83 (90014-02-02-03)	1.5 ± 1.0	0.9 ± 0.6
53293.46 (90014-02-03-00)	1.1 ± 0.1	0.6 ± 0.1
53295.70 (90014-02-03-01)	0.4 ± 0.5	0.2 ± 0.3
From INTEGRAL (JEM-X and IBIS) data		
53273.8 (238)	12.5 ± 1.3	7.4 ± 0.8

a In the 3100 keV energy band.

b In the 3100 keV energy band for an assumed source distance of $d = 7$ kpc.

Naturally, to describe the observed behavior of the pulse profiles more or less accurately, we must complicate significantly the picture described above. Thus, for example, we must know the temperature distribution along the accretion column, the shape of the beam function, its dependence on the object's luminosity, energy band, etc. In addition, since the emission region is close to the neutronstar surface, we must take into account the general relativity effects, which are also capable of affecting the pulse shape (see, e.g., Beloborodov 2002).

The evolution of the pulse profile shape can be clearly illustrated by the intensity maps constructed for the following series of observations: 40411-01-02-00, 40070-01-03-00, 40070-01-05-00, 40051-05-09-00, 40051-05-12-00, and 40051-05-13-00 (see Table 1 and Fig. 2). The maps were obtained by folding the pulsar light curve in narrow (about 4-keV-wide) energy channels whose centroid was displaced from channel to channel by 1 keV. Each profile was constructed in units relative to the mean count rate in a given channel. The resulting map is shown normalized to unity (all intensities were divided by the maximum value over the entire map). The figure shows the maps obtained from PCA and HEXTE data for the first three observations and only from PCA data for the sessions with a lower luminosity. The dashed lines indicate the positions of the fundamental harmonic in the pulsar spectrum (the positions of the first three harmonics for the sessions with a high luminosity). This method of analysis suggested by Tsygankov et al. (2006) when investigating the pulsar V0332+53 allows one to detect and trace large-scale variations in the pulse profile shape with energy and phase. In particular, a "wavy" behavior of the profile shape was found to be observed at all luminosities of the pulsar 4U 0115+63 as the energy varies. The effect lies in the fact that each line of equal intensity of the main peak does not lie at the same phase at different energies, but is slightly displaced alternately in one and another directions. Interestingly, this phase variability of the main peak exhibits a repeatability in energy and its period roughly coincides with the distance between the harmonics of the cyclotron feature in the pulsar spectrum (Fig. 2). As was shown by Tsygankov et al. (2006), the cyclotron feature can affect significantly the pulse profile shape immediately near it. If the observed "waviness" of the pulse profile evolution is assumed to be actually related to the peculiarities of the emission near the cyclotron frequency and its higher harmonics, then one might expect a "wave phase" shift depending on the pulsar luminosity simultaneously with the shift of the cyclotron feature in the spectrum. However, our analysis did not allow us to detect the presence or absence of this shift at a statistically significant level.

The Pulse Fraction

Our intensity maps give a qualitative picture of the pulse profile behavior. To quantitatively describe the observed variations, we used the dependence of the pulse fraction, which is defined as $P = (I_{max} - I_{min})/(I_{max} + I_{min})$, where I_{min} and I_{max} are the background-corrected count rates at the pulse profile minimum and maximum, on energy and luminosity. In all observations, the pulse fraction, on average, increases with energy. The typical energy dependence of the pulse fraction obtained in a wide energy band, 3-100 keV, from PCA/RXTE and HEXTE/RXTE data is shown in Fig. 3 (for the brightest pointing 40070-01-03-00). Figure 4 shows the energy dependences of the pulse fraction for observations with various

pulsar luminosities derived from PCA data in the 3-20 keV energy band; the corresponding luminosities are indicated to the right of each plot. We see that the pulse fraction decreases significantly (from $\sim 65\%$ to $\sim 40\%$ at 10 keV) with increasing luminosity. This result can be explained qualitatively and understood in terms of the simple model suggested above, which describes the luminosity dependence of the pulse profile shape. As the luminosity rises, the geometrical sizes of the emitting regions increase and, accordingly, the pulsations are "smeared". The increase in pulse fraction with energy can also be explained by the fact that the emitting regions are more compact (Fig. 3).

It should be noted that, as we see from Fig. 3 and 4, the pulse fraction increases with energy nonlinearly. The presented dependences exhibit local maxima and minima whose occurrence periodicity roughly coincides with the periodicity of the "wavy" structure of the pulse profile evolution (see above) and may be of the same nature.

To analyze the pulse profile at high energies (above 20 keV) and to investigate the profile evolution with energy, we used IBIS/INTEGRAL observations with a considerably longer exposure time and, accordingly, a better statistical data quality (see Table 2). The vertical dashed lines in the average intensity map constructed from these data (Fig. 5) indicate the centers of the second, third, and fourth cyclotron line harmonics in the pulsar spectrum. We see that the "wavy" structure of the pulse profile evolution with energy noted above based on the RXTE data is also present in a more explicit form in the INTEGRAL data. Nevertheless, whether it is related to the position of the cyclotron line in the source spectrum is still an open question.

Pulse Profile Variability on the Scale of the Pulsation Period

All of the pulse profile properties described above referred to pulses averaged over a long time interval (of the order of several thousand seconds). However, some of the physical and geometrical properties of the emitting regions and their variations can lead to pulse profile variability on time scales shorter than one neutron-star rotation period. In particular, such variability was found in the X-ray pulsar A0535+26. It was shown for this pulsar that the profile-averaged variability cannot be explained only by a Poisson process and that the variability of one of the peaks in the profile is higher than the average variability level over the entire profile (Frontera et al. 1985).

To investigate the profile variations from pulse to pulse, we analyzed the pulsar light curves in various energy channels and at various luminosities. We found that the profile is not stable, but varies significantly on a time scale of the order of the pulsation period. As an example, Fig. 6 shows an arbitrary segment of the source light curve in the 17–20.3 keV energy band for the observing session 40070-01-05-00, when the source luminosity was $\sim 6.6 \times 10^{37}$ erg s^{-1}. The dashed line in the same figure indicates the pulse profile in the same energy band averaged over the entire observing session. We see that the pulse shape is not constant, but changes significantly on the scale of one neutron-star rotation period, while the second peak in the profile (with a lower intensity) exhibits a larger variability in both amplitude and shape.

To quantitatively estimate the pulse profile variability, we analyzed the rms deviation of the count rate in the light curve from the count rate at the corresponding phase of the average profile obtained by folding this light curve with the best period. This quantity (we will call it RMS for short) was calculated as

$$RMS = \frac{\sqrt{\frac{\sum_{k=1}^{N}(P_k - <P_k>)^2 - N\sigma^2}{N}}}{< Flux >}, \quad (1)$$

where P_k is the background-corrected count rate in a given bin of the light curve, $< P_k >$ is the count rate in the bin with the corresponding phase of the averaged profile, N is the total number of bins in the light curve equal to the number of periods that fit in the observation under consideration multiplied by 25 (the number of bins into which each pulse was broken down), σ is the mean measurement error of the count rate in the light curve (this term was introduced to allow for the Poisson noise), and $< Flux >$ is the mean count rate for the entire observation.

The rms deviation RMS obtained in this way reflects the mean variability of the source pulse profile in a given energy band at a given luminosity. To investigate the variability of a particular characteristic feature in the profile, i.e., to analyze the phase dependence of the pulse profile variability, we calculated RMS in a similar way, but the summation was performed only over the bins with the corresponding pulse phases. Figure 7 shows the RMS values obtained in this way divided by the intensity in a given bin of the average profile in four energy bands (upper panels, in %); for comparison, the lower panels show the average pulse profiles in the corresponding energy bands. Such dependences were derived for all observing sessions, but in Fig. 7 we present the results only for two of them (observations 40070-01-03-00 and 40070-01-05-00), when the source was bright enough and a number of characteristic features were present in the pulse profile.

We see from the figure that the ratio of RMS to the intensity in both observations is not constant and behaves in a fairly complex way with pulse phase, but we can distinguish some of its peculiarities (in particular, for session 40070-01-03-00). In all energy bands, the first peak (with a higher intensity) is most stable (the ratio of RMS to the intensity is at a minimum). Its intensity varies insignificantly; only the peak width exhibits a small variability, which is reflected in an increase in RMS in its "wings" (Fig. 7). In contrast, the second peak is much more variable in both amplitude (its variability as a whole is higher than the mean level by several percent) and shape: the corresponding segment of the dependence of RMS on pulse phase (see the upper panels in Fig. 7) manifests itself as a double- or multiple-peaked structure whose variability at maxima is higher than the mean one by 5–10%.

The observed pulse profile variability can be attributed to various physical processes: nonstationarity of the processes in the accretion flow, intensity variability of some nonpulsating continuum, intrinsic variability of the pulse profile, etc. Mathematically, these variability formation mechanisms can be represented as follows:

(i) Multiplicative addition of the variability – the resulting intensity at the current time is defined as $I_1 = \widehat{F}(t) \times P(\varphi)$, where $\widehat{F}(t)$ is a function of only the time and $P(\varphi)$ is the intensity in the averaged profile at phase φ. If only this mechanism were realized, then the ratio of RMS to the intensity of the average profile would be constant.

(ii) Additive addition of the variability, when the intensity is specified as $I_2 = F(t)+P(\varphi)$. In this case, as follows from our definition of RMS, its ratio to the intensity will be inversely proportional to the intensity of the average profile.

As we see from Fig. 7 (and, to some extent, from Fig. 6), the observed variability pattern cannot be fully explained by any of these scenarios, which reflect the effect of only external factors and do not affect the variability of the profile itself, in pure form and by their linear combination. The most generalized case most likely takes place for the pulsar 4U 0115+63.

(iii) $I_3 = F(t) + \widehat{F}(t) \times (P(\varphi) + \widetilde{P}(t, \varphi))$, where $\widetilde{P}(t, \varphi)$ is the component that reflects the processes related to the variation of the pulse profile itself.

As regards the physical causes of the intrinsic profile variability ($\widetilde{P}(t, \varphi)$), apart from the change in the shapes and positions of hot spots on the neutron-star surface (see, e.g., Romanova et al. 2004), the complex structure of the second peak can result from magnetic field multipolarity near the neutron-star surface. The fact that the mean profile variability increases with energy (Fig. 7) can also serve as circumstantial evidence that this variability corresponds to the variability of the accretion flow in the immediate vicinity of the neutron-star surface, where the photon energy is higher.

Thus, the method that we used to analyze the pulse profile shape reveals its "true" variability, which is "blurred" in the average profile, and its stable component. The part of the variability responsible for the "intrinsic" profile variability carries information about specific physical processes in X-ray pulsars and must be taken into account when properly modeling the formation of the pulse profile for such sources.

SPECTRAL ANALYSIS

To describe the source spectrum, we used a combination of models that consisted of a power law and a high-energy cutoff (the powerlaw*highecut model in the XSPEC package; White et al. 1983) modified by absorption lines in the shape of a Lorenz profile, $exp\left(\frac{-\tau_{cycl}(E/E_{cycl})^2\sigma^2_{cycl}}{(E-E_{cycl})^2+\sigma^2_{cycl}}\right)$, where E_{cycl} is the energy of the line center, τ_{cycl} is the line depth, and σ_{cycl} is the line width. The fluorescent iron line at 6.4 keV was also detected in the spectrum when fitting the data obtained in observations with a high emission intensity.

It should be noted that whether the iron emission line is present in the source spectrum is still an open question. In several papers (Tamura et al. 1992; Nakajima et al. 2006), it was not required to include this feature in the model to satisfactorily describe the experimental data. In contrast, another group of authors (Nagase et al. 1991; Lutovinov et al. 2000; Mihara et al. 2004) detected this feature at a statistically significant level. This ambiguity

results from the fact that the analytical model used is complex and somewhat "artificial" and that the cutoff energy in the source spectrum E_{cut} is close to the line energy. The final conclusion about the presence of this feature in the pulsar spectrum is difficult to reach, but its inclusion in the fitting model reduces significantly the χ^2 value. The line equivalent width for different observations changes from $\sim$ 150 eV in a state with a high luminosity to $\sim$ 50 eV in a state with a low luminosity. This value is compatible with the situation where the "cold" matter behind the X-ray source (e.g., the matter flowing over the neutron-star magnetosphere or the bent edge of the accretion disk) intercepts and reradiates in the observer's direction about half of the incident emission (George and Fabian 1991). Based on this fact, we can interpret the decrease in the iron line equivalent width with declining luminosity as a decrease in the area of the reflecting surface. Much information about the geometry of reflecting regions and, in particular, the distances to them can be obtained by analyzing the behavior of the iron line with pulse phase. However, due to the complex shape of the spectrum and the relatively low intensity of this line, observations with a high energy resolution near 6.4 keV are required to detect it.

Figure 8 shows the source spectrum in a wide energy band obtained from INTEGRAL data. Note that the quality of the fit to the experimental data at energies below 20 keV is not ideal; in particular, this may stem from the fact that the JEM-X response matrix is imperfect (for comments, see Filippova et al. 2005). The parameters of the model consisting of a power law with a high-energy cutoff and four cyclotron line harmonics are given in Table. 3.

Table 3. Spectral parameters of 4U 0115+63 with INTEGRAL.

Model parameters	Value
Photon index	$0.093^{+0.007}_{-0.001}$
E_{cut}, keV	8.93 ± 0.03
E_{fold}, keV	$9.06^{+0.09}_{-0.02}$
$\tau_{cycl,1}$	0.55 ± 0.01
$E_{cycl,1}$, keV	$11.16^{+0.03}_{-0.02}$
$\sigma_{cycl,1}$, keV	$3.13^{+0.07}_{-0.02}$
$\tau_{cycl,2}$	0.97 ± 0.01
$E_{cycl,2}$, keV	$21.16^{+0.11}_{-0.02}$
$\sigma_{cycl,2}$, keV	$7.55^{+0.15}_{-0.02}$
$\tau_{cycl,3}$	0.40 ± 0.01
$E_{cycl,3}$, keV	$34.55^{+0.01}_{-0.20}$
$\sigma_{cycl,3}$, keV	$4.5^{+0.3}_{-0.1}$
$\tau_{cycl,4}$	0.55 ± 0.01
$E_{cycl,4}$, keV	$44.93^{+0.15}_{-0.27}$
$\sigma_{cycl,4}$, keV	$11.38^{+0.45}_{-0.17}$
E_{Fe}, keV	6.4 fixed
σ_{Fe}, keV	0.2 fixed
EW_{Fe}, eV	130 ± 10
χ^2 (d.o.f)	0.85(155)

The derived model parameters agree with the results obtained from RXTE data and earlier by other authors.

The characteristic source energy spectrum obtained in two observations with different luminosities and cyclotron energies (observations 40070-01-05-00 and 40051-05-09-00) from PCA data are shown in Fig. 9.

Luminosity Dependence of the Cyclotron Line Energy

Mihara et al. (1998) and Nakajima et al. (2006) showed that the position of the cyclotron absorption line changes with pulsar luminosity from ~ 11 keV near the outburst maximum to ~ 16 keV at the end of the outburst, when the source luminosity falls by more than an order of magnitude. If the observed emission at the end of the outburst is assumed to originate mainly near the neutron-star surface, then we can estimate the magnetic field of 1he neutron star, $B = (1+z) \times E_{cycl} \times 10^{12}/11.6 \simeq 1.4 \times 10^{12}$ G. Nevertheless, although the pulsar properties have long been studied, the cyclotron frequency variation with source luminosity is not completely clear. Below, we investigate this transition during the 2004 outburst; for comparison, we also analyze the data for the 1999 outburst.

Figures 10 and 11 show the time dependences of the luminosity (open squares) and position of the fundamental cyclotron frequency harmonic (the filled squares and triangles for the 1999 and 2004 outbursts, respectively). It is clearly seen from the figures that the cyclotron energy at high luminosities ($\sim 10^{38}$ erg s^{-1}) lies within the range $\sim 10-11$ keV and is virtually independent of the pulsar emission intensity. As the luminosity decreases to $\sim 5 \times 10^{37}$ erg s^{-1}, the cyclotron energy increases sharply to ~ 14 keV, with its small rise to $\sim 15-16$ keV as the source luminosity decreases further.

The cyclotron frequency is plotted against the intrinsic luminosity in Fig. 12 based on RXTE (the designations are the same as those in Figs. 10 and 11) and INTEGRAL (filled circle) data. We see that the results obtained with different instruments and during different outbursts are in good agreement. In both cases, the cyclotron line energy changes sharply at the same luminosity ($\sim 5 \times 10^{37}$ erg s^{-1}), suggesting that the observed jump is probably a fundamental property of the pulsar under study. Searching for and investigating of such a transition at the outburst rise phase are of great interest. However, the observations during both outbursts were begun too late and the characteristic luminosity at which the jump in cyclotron line energy is detected was not observed at the rise phase.

Assuming a dipole magnetic field configuration, a relative change in the fundamental harmonic energy $\Delta E_{cyc}/E_{cyc} \sim 60\%$ corresponds to a relative change in its formation height $\Delta R/R \sim 20\%$, which is equivalent to a change in the radius by ~ 2 km (taking the neutron-star radius to be 10 km).

By studying the spectral characteristics of the emission at a certain source luminosity, we can obtain constraints on the height of the accretion column segment where this emission is generated effectively. To a first approximation, the electron energy (Landau) levels at a given magnetic field strength may be assumed to be arranged according to the harmonic law (1:2:3...). The model by Basko and Sunyaev (1976) predicts that harder radiation in the

accretion column emerges from regions closer to the neutron-star surface, where the magnetic field strength is higher. Thus, the deviations of the energies of the fundamental and higher harmonics in the spectrum of 4U 0115+63 from a linear law can be used to compare the effective sizes of the emitting regions at $\sim$ 11, 22, 33, and 44 keV, respectively. The energies of the higher harmonics should lie above the harmonic law. Figure 13 illustrates the picture described above for the observations with luminosities of 7.4×10^{37} erg s^{-1} from INTEGRAL data (filled squares and thick lines) and 11.0×10^{37} erg s^{-1} from RXTE data (open circles and thin lines). Based on the energy of the fundamental cyclotron line harmonic, we determined the harmonic law (dotted lines) and analyzed the deviations of the centroids of the higher harmonics from it. Since the formal statistical errors in the line centroid are much smaller than the energy resolution of the instruments used, we introduced a systematic uncertainty at the level of a characteristic scatter of values ($\sim$ 1 keV). For this purpose, 0.5 keV was added quadratically to the statistical error.

To determine the possible scatter of heights in the accretion column by the method described above, we took the observed deviations of the centroid energies for the higher cyclotron line harmonics from the harmonic law indicated by the dashed line. Given the possible statistical and systematic errors, the maximum possible deviation from the harmonic law that is formally compatible with the observational data is indicated in the figure by the solid lines for each observation. This maximum deviation specifies the most conservative constraint on the deviation from the harmonic law. As a result, the observed deviation from the harmonic law at a luminosity of 7.4×10^{37} erg s^{-1} (INTEGRAL data) was found to be $\Delta E_{cyc}/E_{cyc}\sim 1\%\pm3\%$ at the energy of the highest observable (fourth) cyclotron line harmonic ($\sim$ 45 keV). Note that, given the measurement errors, this result is completely compatible with a purely harmonic dependence of the line centroid positions. In terms of the effective heights of the emitting regions (at energies $\sim$ 11, 22, 33, and 44 keV), these deviations correspond to $\Delta R/R\sim0.3\%\pm1\%$. The most conservative estimate yields $\Delta E_{cyc}/E_{cyc}<9\%$ and $\Delta R<300$ m. Consequently, the effective sizes of the emitting regions in this state do not differ by more than several hundred meters and this difference is most likely even smaller.

For the other observation (at a higher luminosity, 11.0×10^{37} erg s^{-1}, RXTE observations), the observed deviation from the harmonic law is $\Delta E_{cyc}/E_{cyc}\sim16\%\pm3\%$ at the energy of the highest observable (third) cyclotron line harmonic ($\sim$ 36 keV), while the corresponding most conservative limit is $\Delta E_{cyc}/E_{cyc}<26\%$ ($\Delta R<900$ m). We see from the figure that in this case the higher harmonics actually have energies above the harmonic law, as might be expected at an appreciable linear size of the column and a dependence of the hardness of the emergent photons on the distance to the stellar surface.

For the first observation (at a luminosity 7.4×10^{37} erg s^{-1} appreciably lower than the maximum one), the small deviations from the harmonic law can be interpreted as resulting from the fact that the emitting region is compact or that the hardness of the emergent photons does not depend on the distance to the stellar surface. Interestingly, the constraints on the scatter ΔR are considerably smaller than the estimate obtained by assuming that the abrupt change in cyclotron frequency (at a luminosity of $\sim5\times10^{37}$ erg s^{-1}) is related to a

change in the height of the shock wave in the accretion column.

At fairly high harmonic energies, the relativistic corrections to the harmonic law may prove to be significant (Harding and Daugherty 1991). The correction is $\frac{1}{2}\frac{E}{m_e c^2}$ in order of magnitude, i.e., does not exceed 4% for the maximum cyclotron line energy of ∼45 keV observed for the source 4U 0115+63. Therefore, the relativistic corrections have virtually no effect on the conclusions reached above.

Constancy of the Cutoff energy (E_{cut}) in the Source Spectrum

Another distinctive feature of the pulsar 4U 0115+63 is the stability of its spectral shape during an outburst. In particular, the cutoff energy in the spectrum (E_{cut}) does not correlate with the cyclotron frequency and, being fixed at 8.9 keV, it distorts only slightly the other parameters of the fit and does not deteriorate the χ^2 value. As an example, let us consider two RXTE observations, 40051-05-05-00 and 40051-05-09-00, when the energies of the fundamental cyclotron line harmonic were ~ 10.7 and ~ 14.9 keV, respectively. Thus, if we fit the chosen sessions by a model where the cutoff energy E_{cut} is a free parameter, then the total $\chi^2(N)$ value (with N degrees of freedom) will be 16.58(36) and 26.08(36), respectively. If, however, E_{cut} is fixed at 8.9 keV, then the $\chi^2(N)$ values will be 17.16(37) and 26.30(37), respectively. This result is interesting in that it allows us to test the assumption that the cutoff energy in the spectrum depends on the cyclotron energy. A correlation between these parameters derived from the average spectra of various sources was found in a number of papers (see, e.g., Makishima et al. 1999; Orlandini and Dal Fiume 2001; Coburn et al. 2002). Because of the wide dynamic range of the relative change in cyclotron energy for the source under study ($\sim 50\%$), we can check whether this correlation exists not for different sources, but for the same pulsar. Using the same set of observations (40051-05-05-00 and 40051-05-09-00) and assuming that the cutoff energy in the spectrum in a brighter state (40051-05-05-00) is ~ 8.9 keV, E_{cut} in the fitting model of the second spectrum was specified to be proportional to the cyclotron energy. As a result, the quality of the fit proved to be unacceptable, which, in particular, manifests itself in a sharp increase in $\chi^2(N)$ (57.35(37)).

Since E_{cut} and the remaining parameters of the fitting model remain essentially constant, we can assume that the cutoff energy depends not on the instantaneous cyclotron energy (i.e., on the specific configuration of the accretion regions at the poles), but rather reflects the fundamental properties of the neutron star. For example, when analyzing the observations of the X-ray pulsar Her X-1, Gruber et al. (2001) found the cyclotron energy in the source spectrum to increase. This was interpreted as a change in the magnetic field strength of the neutron star. In this case, a direct proportionality between the cutoff energy (E_{cut}) and the cyclotron frequency was observed.

CONCLUSIONS

We investigated the accreting X-ray pulsar 4U 0115+63 using the RXTE and INTEGRAL data obtained during intense outbursts in 1999 and 2004. Below, we briefly summarize the most interesting and important results.

– We analyzed the dependence of the pulse profile on the source luminosity; we showed that the intensity of the second peak in the profile decreases with declining source luminosity as well as with increasing energy and the peak disappears almost completely at energies above ~ 20 keV. We suggested a model describing qualitatively this behavior of the profile in which the lower part of one of the accretion columns (emitting harder photons) is partially screened from the observer by the neutron star surface; as the source luminosity declines, the column height decreases and an increasingly large part of it is screened from the observer.

– The pulse fraction was shown to increase both with decreasing intrinsic source luminosity and with increasing energy. This suggests that the hard X-ray emitting regions are more compact, which is compatible with the model described above. On the scale of the pulsar period, we revealed a component in the variability of the pulse profile shape that is not described by the accretion flow variability, but is related to the intrinsic variability of the pulse profile.

– We detected a cyclotron absorption line and its three higher harmonics in the pulsar spectrum. We analyzed the dependence of the cyclotron absorption line energy on the pulsar luminosity and showed that this dependence is nonlinear and that the line energy increases abruptly when the source reaches a luminosity of $\sim 5 \times 10^{37}$ erg s^{-1}. The possible scatter of heights at which emission with different energies is produced in the accretion column was estimated from the deviations of the centroids of the higher cyclotron line harmonics from an equidistant distribution.

– We showed that the cutoff energy in the spectrum is be essentially constant during an outburst and does not correlate with the cyclotron energy.

ACKNOWLEDGMENTS

We thank M.G. Revnivtsev for help with the RXTE data analysis and for a discussion of the results obtained. This work was supported by the Ministry of Industry and Science (Presidential grant RF NSh-1100.2006.2), the "Origin and Evolution of Stars and Galaxies" Program of the Presidium of the Russian Academy of Sciences, and the Russian Foundation for Basic Research (projects no. 05-02-17465 and 07-02-01051). A.A. Lutovinov thanks the Russian Science Support Foundation. We used data from the High Energy Astrophysics Science Archive Research Center Online Service provided by the NASA/Goddard Space Flight Center, the INTEGRAL Science Data Center (Versoix, Switzerland), and the Russian INTEGRAL Science Data Center (Moscow, Russia).

Basko M.M., Sunyaev R.A., Mon. Not. Roy. Astron. Soc. **175**, 395 (1976)

Beloborodov A.M., Astrophys. J. **566**, L85 (2002)

Bradt H.V., Rothschild R.E., Swank J.H., Astron. Astrophys. Suppl. Ser. **97**, 355 (1993)

Coburn W., Heindl W., Rothschild R. *et al.*, // Astrophys. J. **580**, 394 (2002)

Cominsky L., Clark G.W., Li F. *et al.*, Nature **273**, 367 (1978)

Filippova E., Tsygankov S., Lutovinov A., Sunyaev R., Astron. Lett., **31**, 729 (2005)

Forman W., Jones C., Cominsky L. *et al.*, Astrophys. J. Suppl. Ser. **38**, 357 (1978)

Frontera F., dal Fiume D., Morelli E., Spada G., Astrophys. J. **298**, 585 (1985)

Gruber D. E., Heindl W. A., Rothschild R. E. *et al.*, Astrophys. J. **562**, 499 (2001)

Giacconi R., Murray S., Gursky H. *et al.*, Astrophys. J. **178**, 281 (1972)

George I.M., Fabian A.C., Mon. Not. Roy. Astron. Soc. **249**, 352 (1991)

Harding A.K., Daugherty J.K., Astrophys. J. **374**, 687 (1991)

Heindl W.A., Coburn W., Gruber D.E. *et al.*, Astrophys. J. **521**, L49 (1999)

Hutchings J.B., Crampton D., Astrophys. J. **247**, 222 (1981)

Kholopov P.N., Samus N.N., Kukarkina N.P. *et al.*, Information Bulletin on Variable Stars, 2042, 1 (1981)

Lebrun F., Leray J. P., Lavocat P. *et al.*, Astron. Astrophys. **411**, L141 (2003)

Lund N., Brandt S., Budtz-Joergesen C. *et al.*, Astron. Astrophys. **411**, L231 (2003)

Lutovinov A. A., Grebenev S. A., Syunyaev R. A., Pavlinskii M. N., Astron. Lett., **20**, 538 (1994)

Lutovinov A. A., Grebenev S. A., Sunyaev R. A., Astron. Lett., **26**, 1 (2000)

Lutovinov A., C.Budtz-Jorgensen, M.Turler *et al.*, The Astronomers Telegram **326** (2004)

Makishima K., Mihara T., Nagase F., Tanaka Y., Astrophys. J. **525**, 978 (1999)

Mihara T., Makishima K., Nagase F., Adv. Space Res. **22**, 987 (1998)

Mihara T., Makishima K., Nagase F., Astrophys. J. **610**, 390 (2004)

Mineo T., Ferrigno C., Foschini L. *et al.*, Astron. Astrophys. **450**, 617 (2006)

Nagase F., Dotani T., Tanaka Y. *et al.*, Astrophys. J. **375**, L49 (1991)

Nakajima M., Mihara T., Makishima K., Niko H., Astrophys. J. **646**, 1125 (2006)

Negueruela I., Okazaki A.T., Astron. Astrophys. **369**, 108 (2001)

Orlandini M., Fiume D.Dal, AIP Conference Proceedings **599**, 283 (2001)

Rappaport S., Clark G.W., Cominsky L. *et al.*, Astrophys. J. **224**, L1 (1978)

Revnivtsev M., Sunyaev R., Varshalovich D., et al., Astron. Lett., **30**, 382 (2004)

Romanova M. M., Ustyugova G. V., Koldoba A. V., Lovelace R. V. E., Astrophys. J. **610**, 920 (2004)

Santangelo A., Segreto A., Giarrusso, S. *et al.*, Astrophys. J. **523**, L85 (1999)

Tamura K., Tsunemi H., Kitamoto S. *et al.*, Astrophys. J. **389**, 676 (1992)

Tsygankov S., Lutovinov A., Churazov E., Sunyaev R., Mon. Not. Roy. Astron. Soc. **371**, 19 (2006)

White N., Swank J., Holt S., Astrophys. J. **270**, 771 (1983)

Wheaton W. A., Doty J. P., Primini F. A. *et al.*, Nature **282**, 240 (1979)

Winkler C., Courvoisier T.J.-L., Di Cocco G. *et al.*, Astron. Astrophys. **411**, L1 (2003)

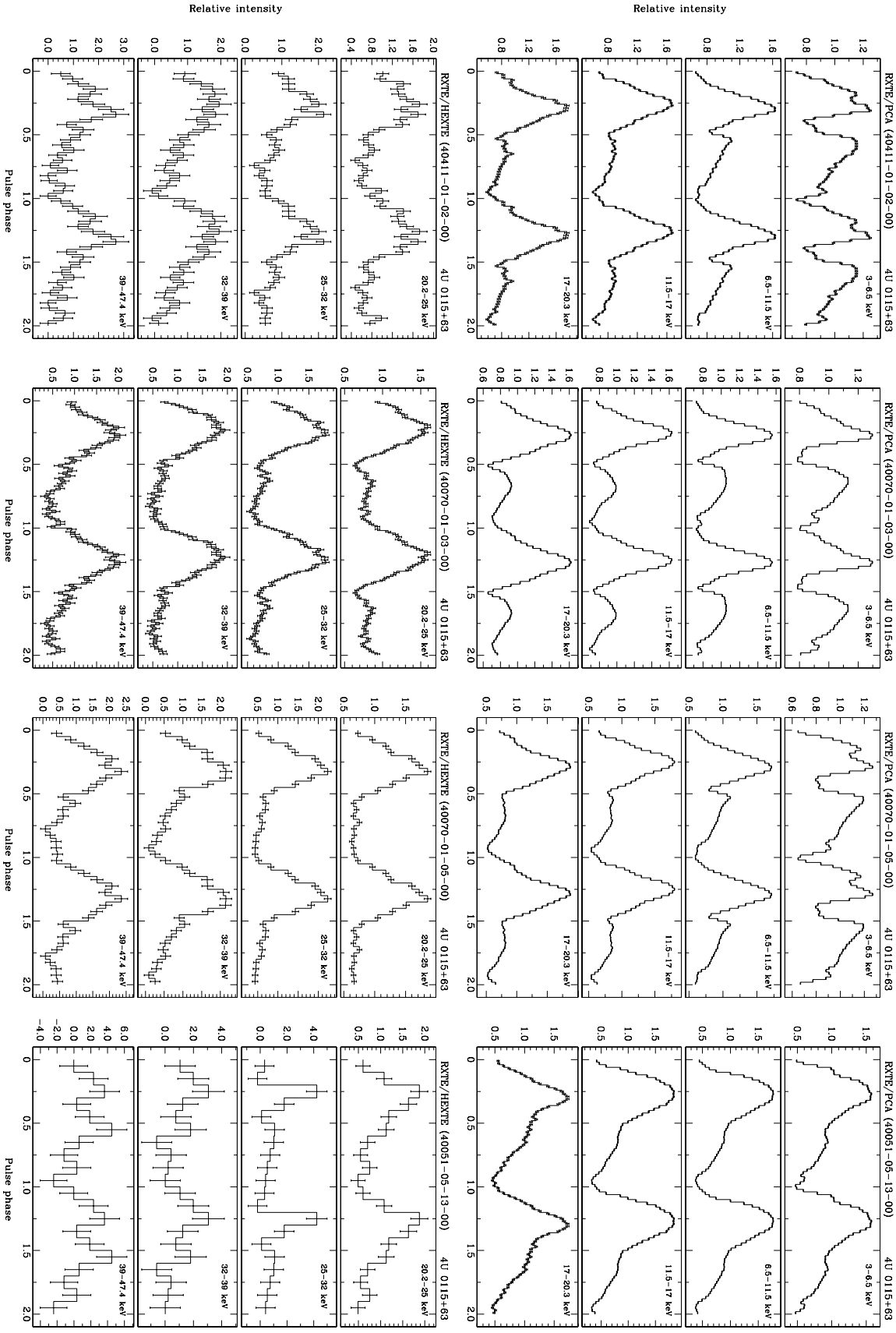

Fig. 1: Pulse profile shape as a function of the source luminosity and energy band. The columns are arranged from the outburst onset from left to right and correspond to luminosities $\sim 7.3\times10^{37}$, $\sim 14.6\times10^{37}$, $\sim 6.6\times10^{37}$, $\sim 1.5\times10^{37}$ erg s^{-1}. The background was subtracted.

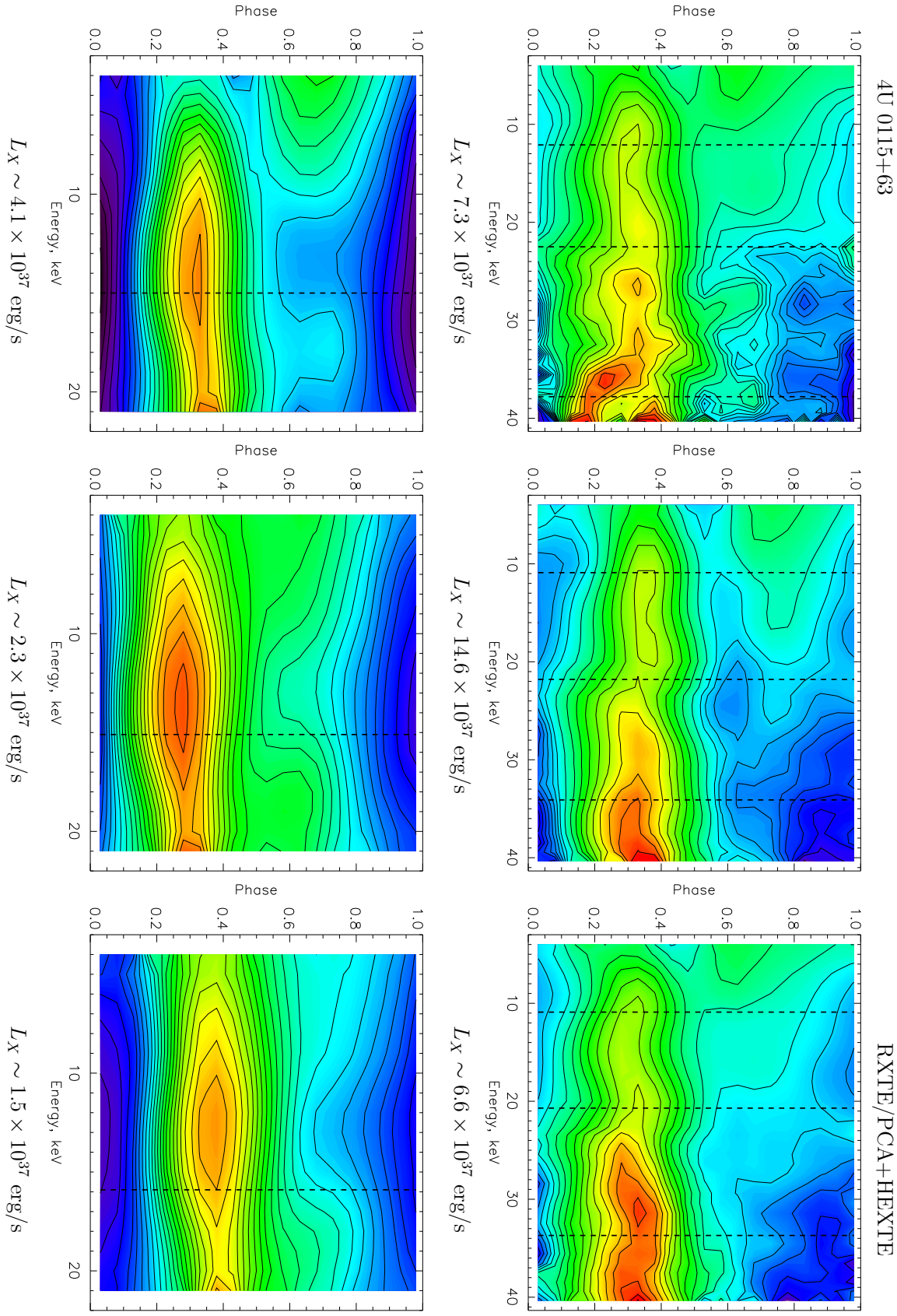

Fig. 2: Background-corrected intensity maps of the pulse profile for the X-ray pulsar 4U 0115+63 from PCA/RXTE and HEXTE/RXTE data as a function of the energy band and source bolometric luminosity (see the text). The dashed lines indicate the positions of the cyclotron frequency harmonics in the source spectrum; the corresponding source luminosities are given under the maps.

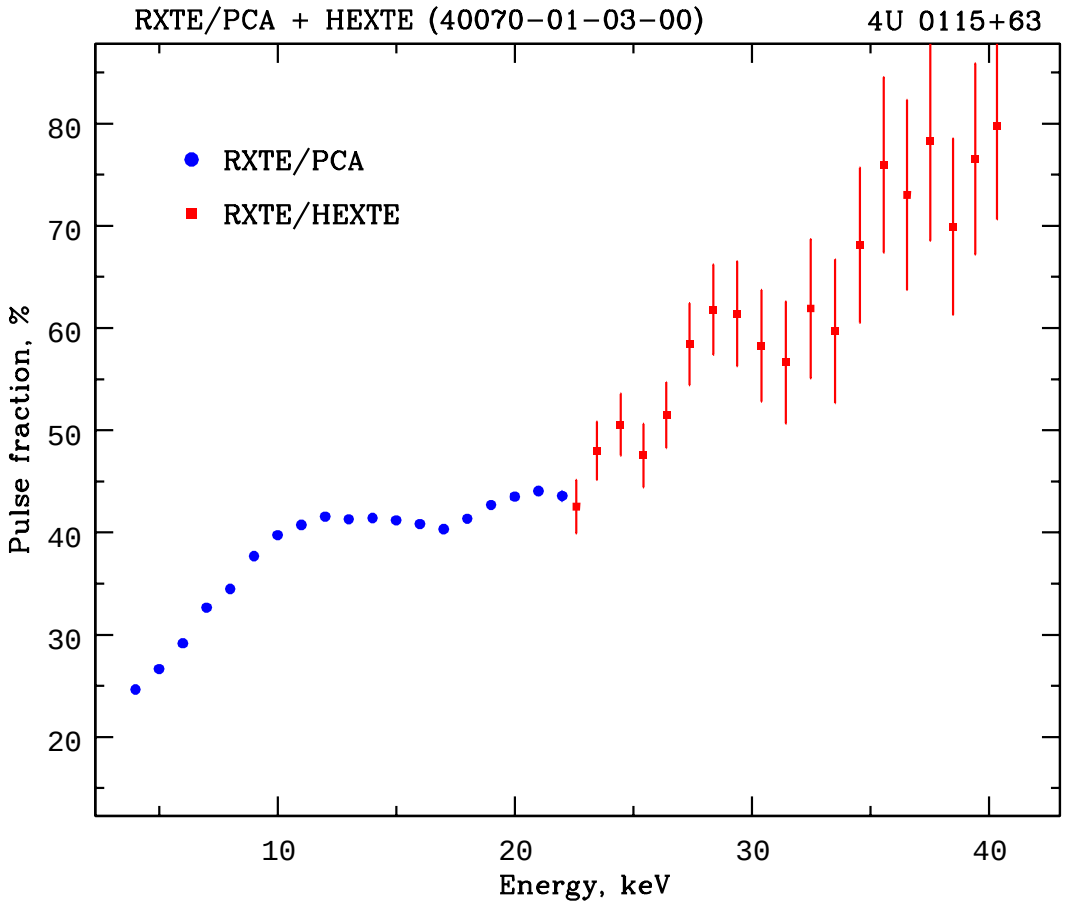

Fig. 3: Pulse fraction versus energy from the RXTE data obtained during the 1999 outburst, when the pulsar luminosity was at a maximum (observation 40070-01-03-00).

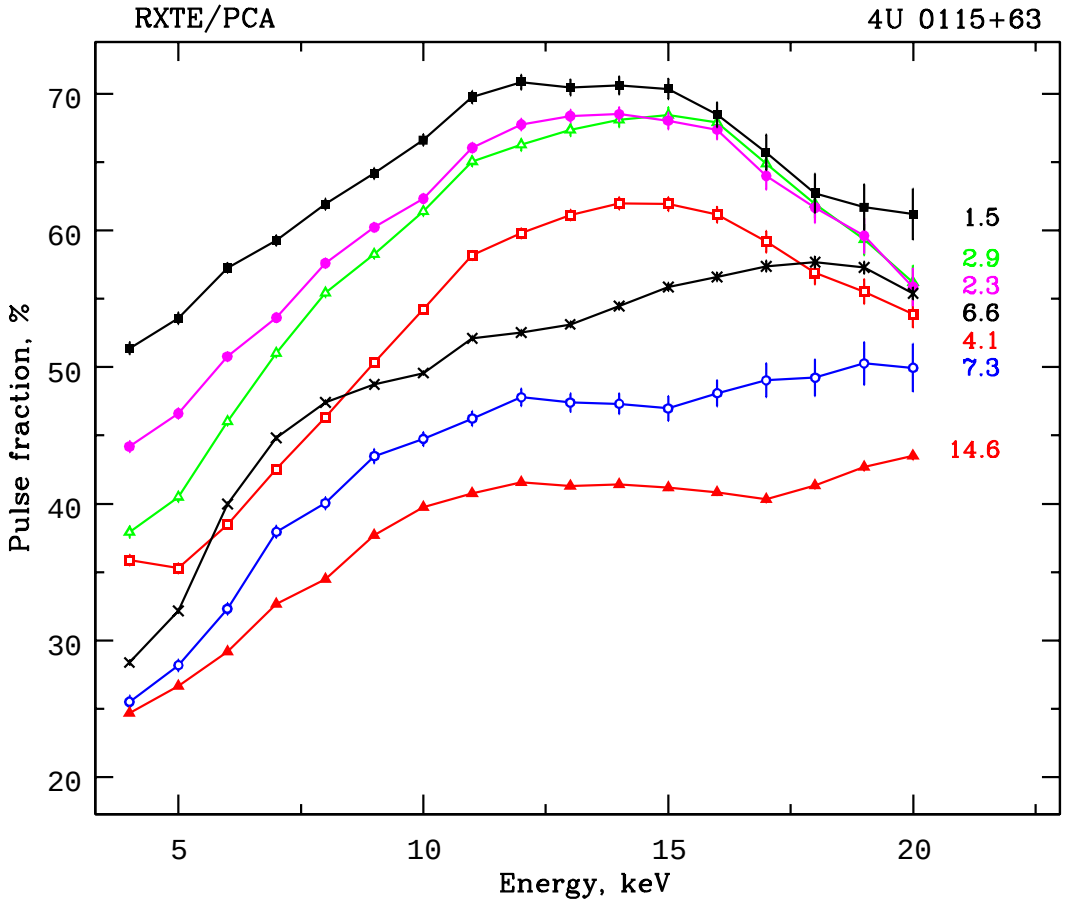

Fig. 4: Pulse fraction versus energy for various bolometric luminosities of the pulsar (shown to the right of the corresponding curves in units of 10^{37} erg s^{-1}) from PCA/RXTE data.

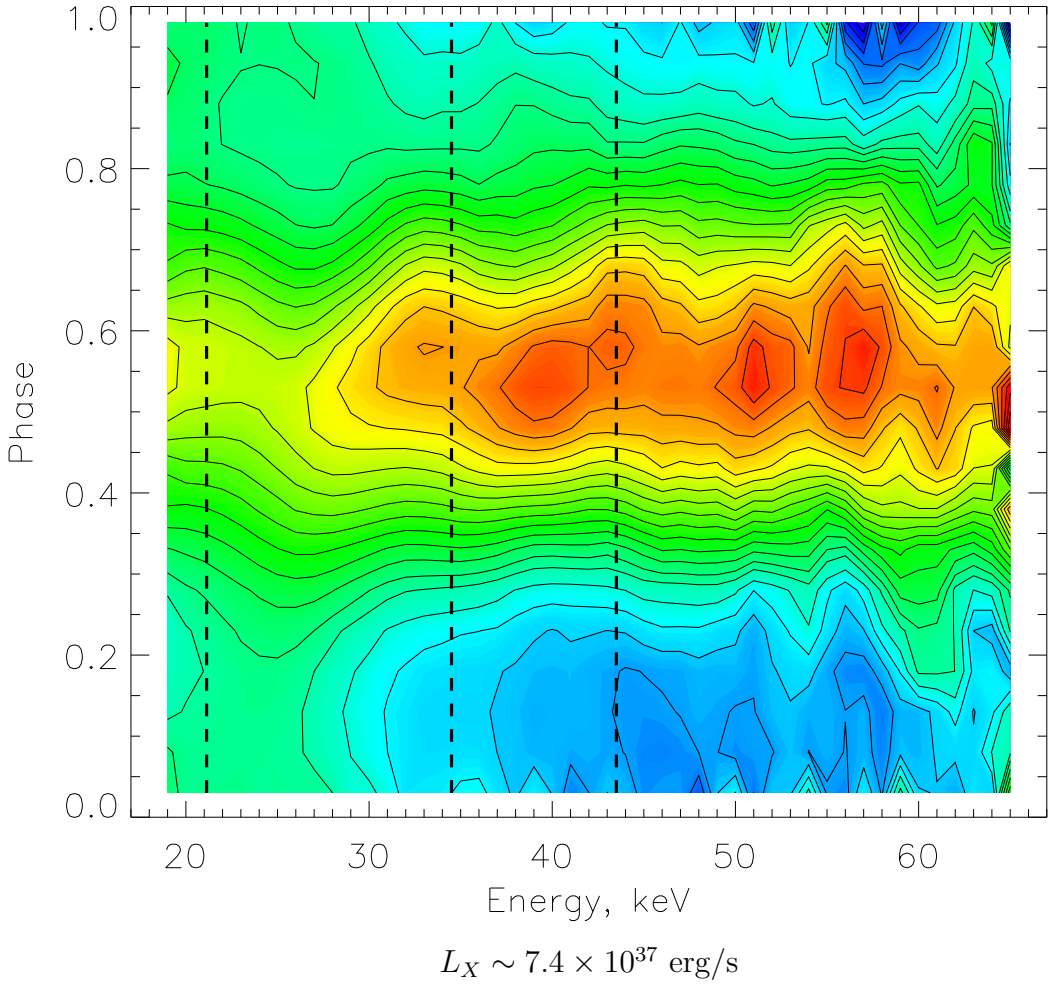

Fig. 5: Background-corrected intensity map of the pulse profile for the X-ray pulsar 4U 0115+63 from IBIS/INTEGRAL data. The source luminosity in this observation is $\sim 7.4 \times 10^{37}$ erg s^{-1}. The dashed lines indicate the positions of the second, third, and fourth cyclotron frequency harmonics in the source spectrum.

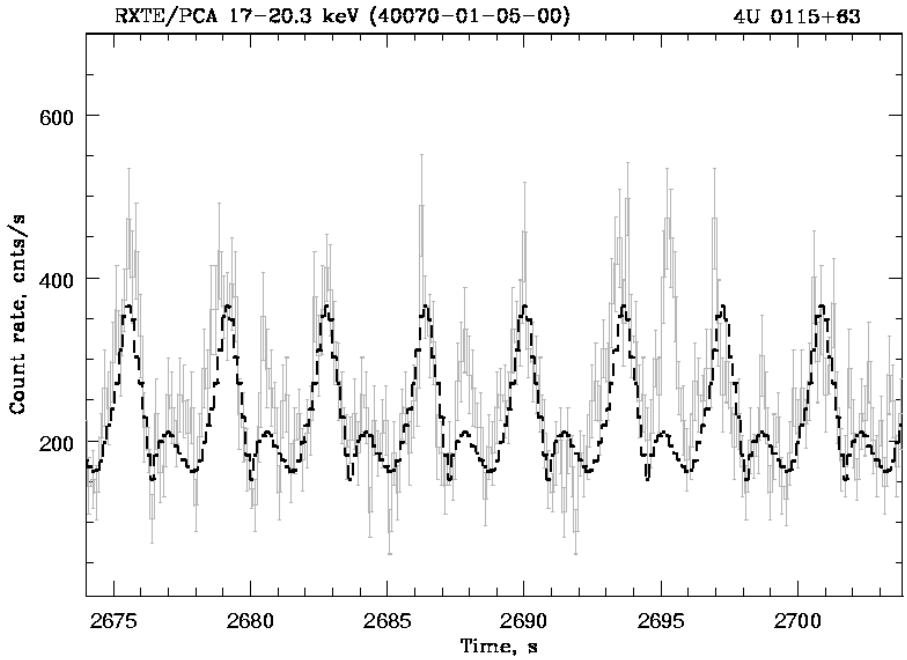

Fig. 6: Pulsar 1720.3 keV light curve at a luminosity of $\sim 6.6 \times 10^{37}$ erg s^{-1} (observation 40070-01-05-00). The dashed line indicates the average pulse profile shape in this energy band for the entire observing session. The background was subtracted.

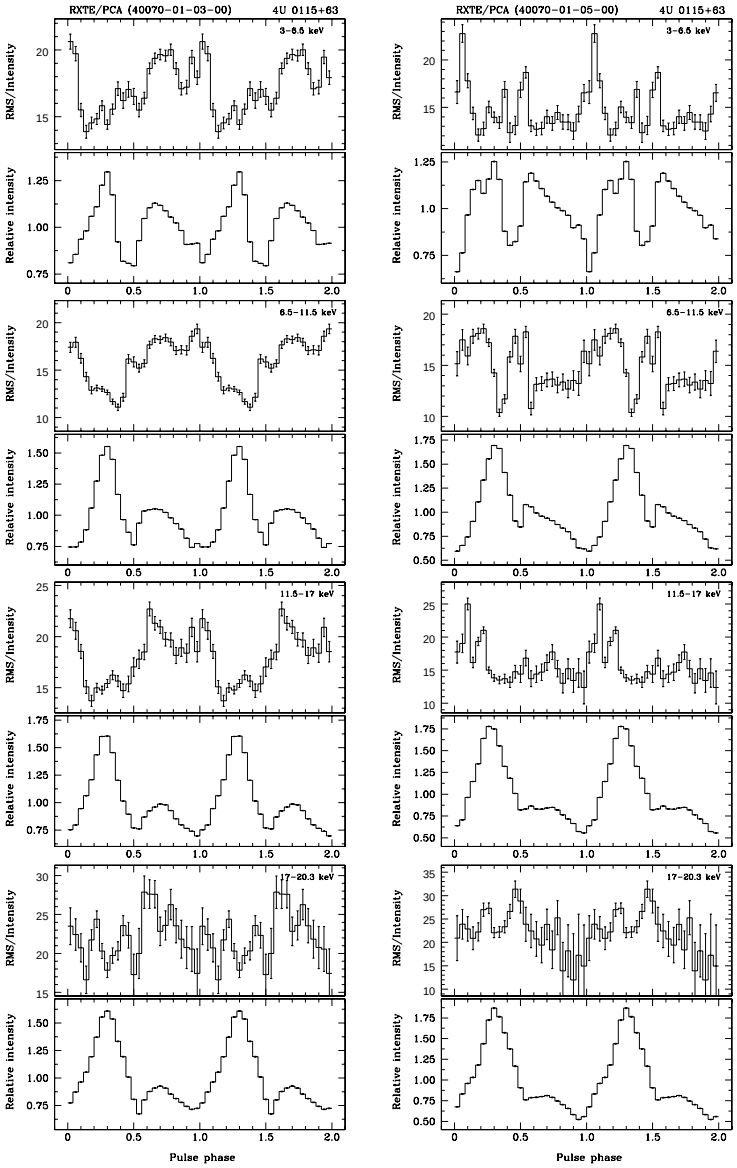

Fig. 7: Rms deviation (RMS , see the text) divided by the count rate in the average pulse profile versus pulse phase (upper panels) for two source luminosities ($\sim 14.6\times10^{37}$ and $\sim 6.6 \times 10^{37}$ erg s^{-1}) in various energy bands. For comparison, the lower panels show the average pulse profiles in the corresponding energy bands for the observations under consideration.

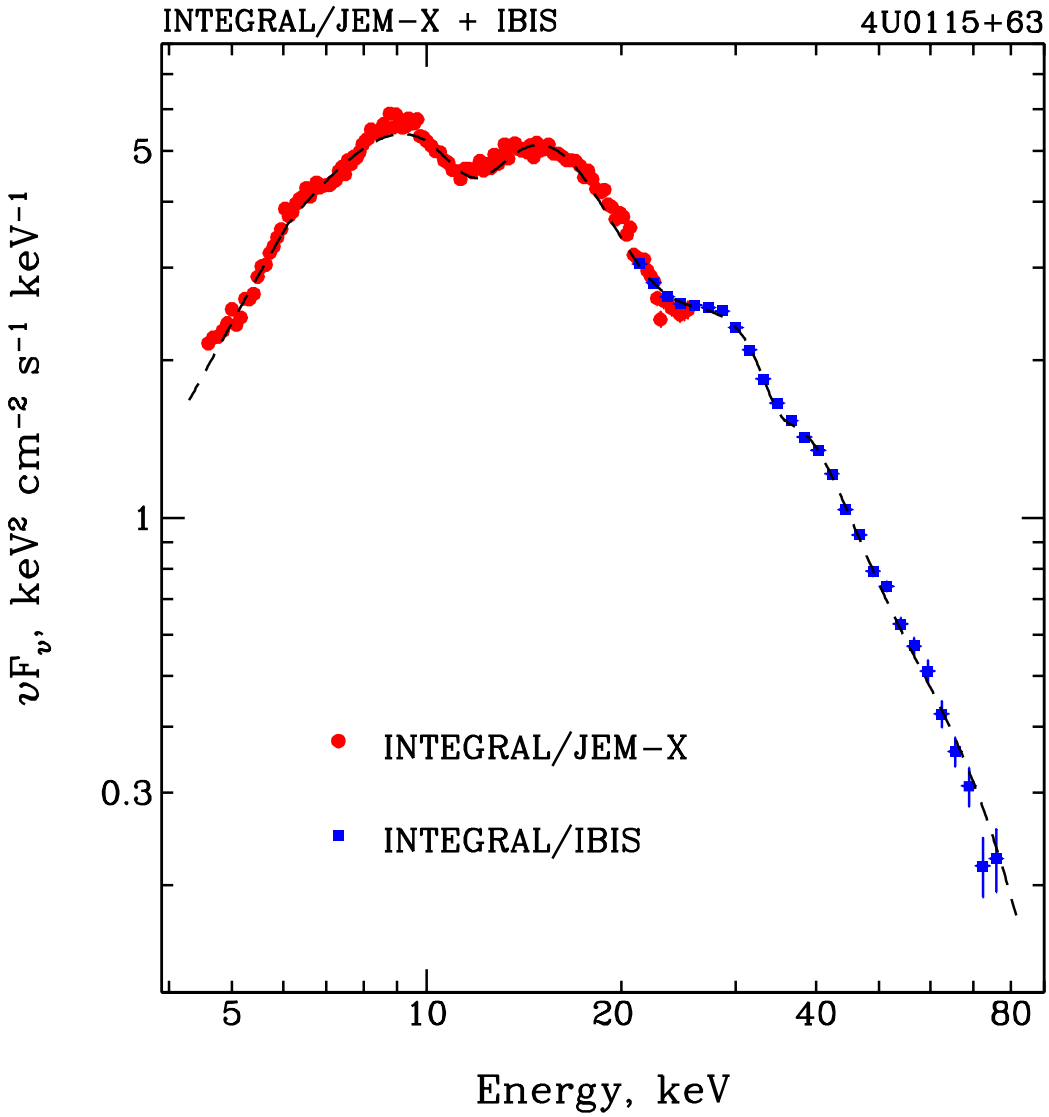

Fig. 8: Pulsar energy spectrum from INTEGRAL data in a wide energy band. The model (dashed line) does not include the component related to the iron emission line (see the text).

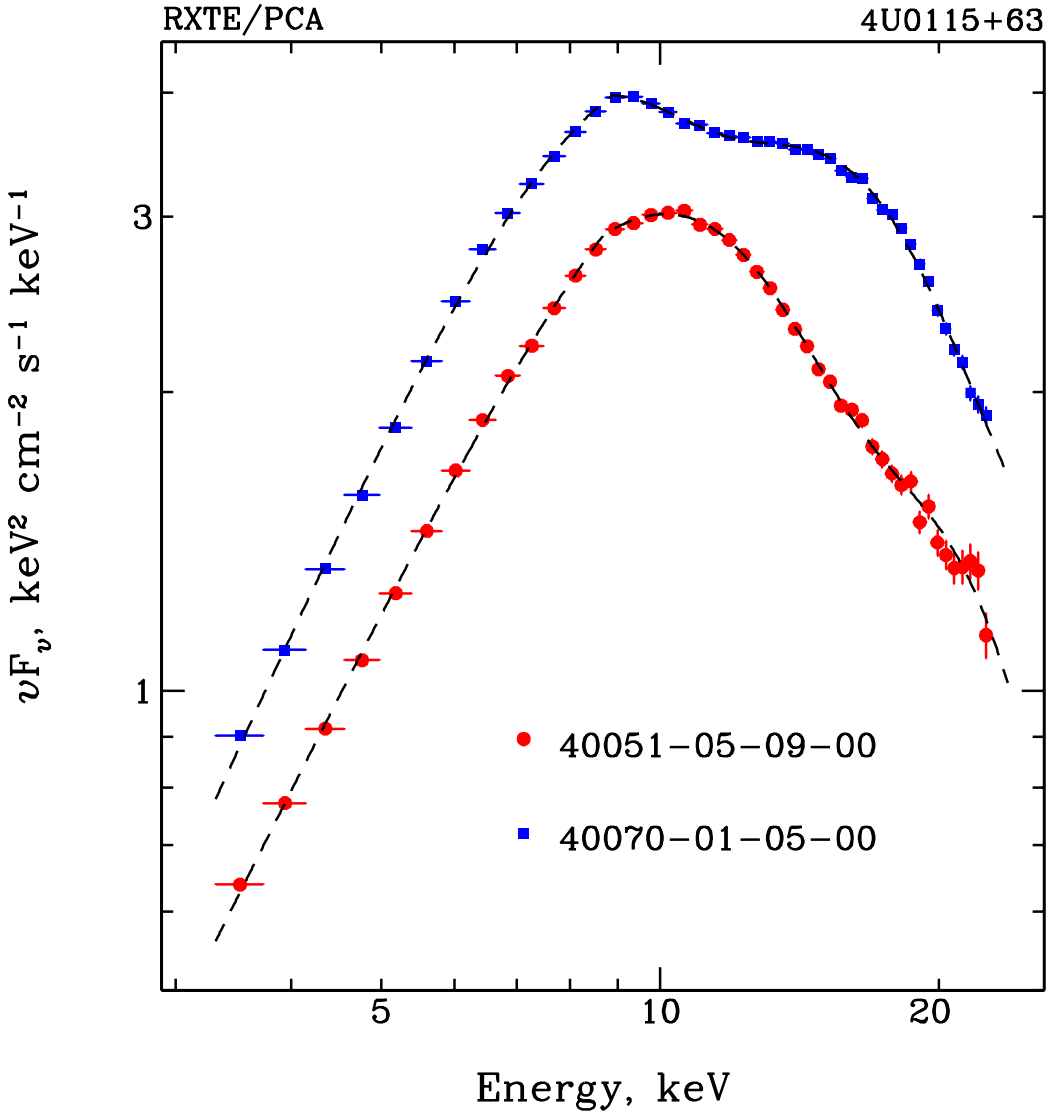

Fig. 9: Characteristic energy spectra of the source in states with different luminosities ($\sim 6.6\times10^{37}$ and $\sim 4.1\times10^{37}$ erg s^{-1}) from PCA/RXTE data. The fitting model (dashed lines) does not include the component related to the iron emission line.

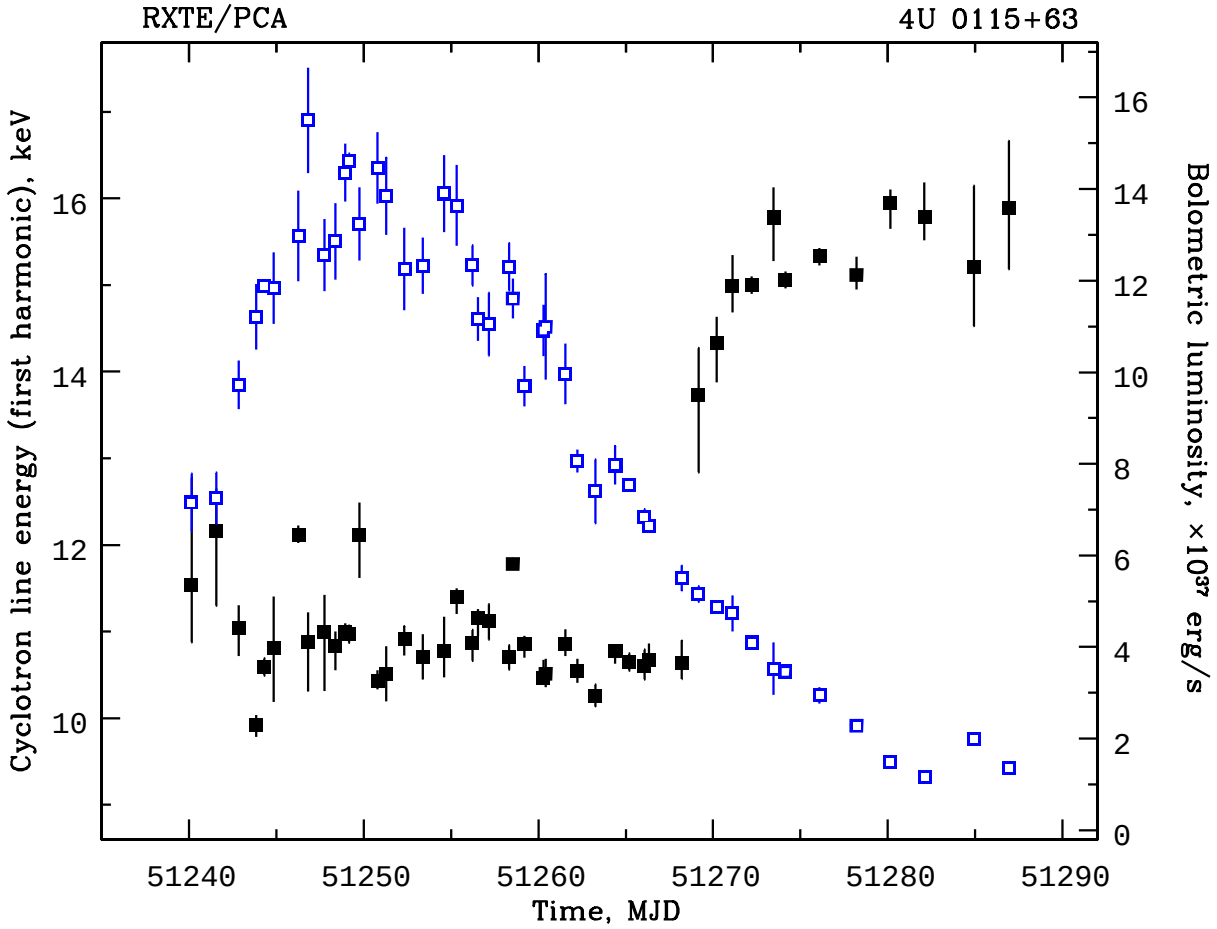

Fig. 10: Position of the fundamental harmonic of the cyclotron absorption line in the pulsar spectrum (filled squares) and $3-100$ keV luminosity (open squares) as a function of time from the RXTE data in 1999.

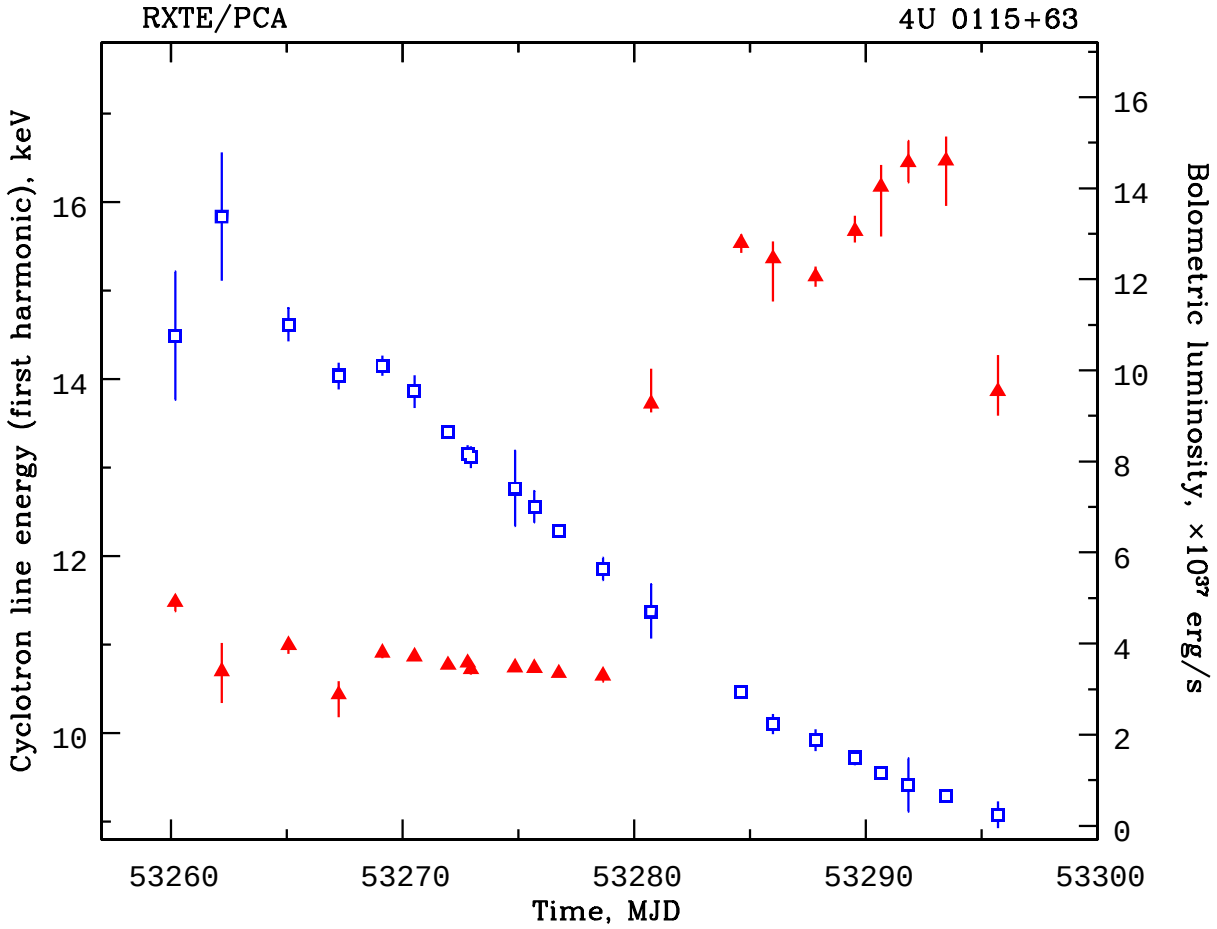

Fig. 11: Position of the fundamental harmonic of the cyclotron absorption line in the pulsar spectrum (filled triangles) and $3-100$ keV luminosity (open squares) as a function of time from the RXTE data in 2004.

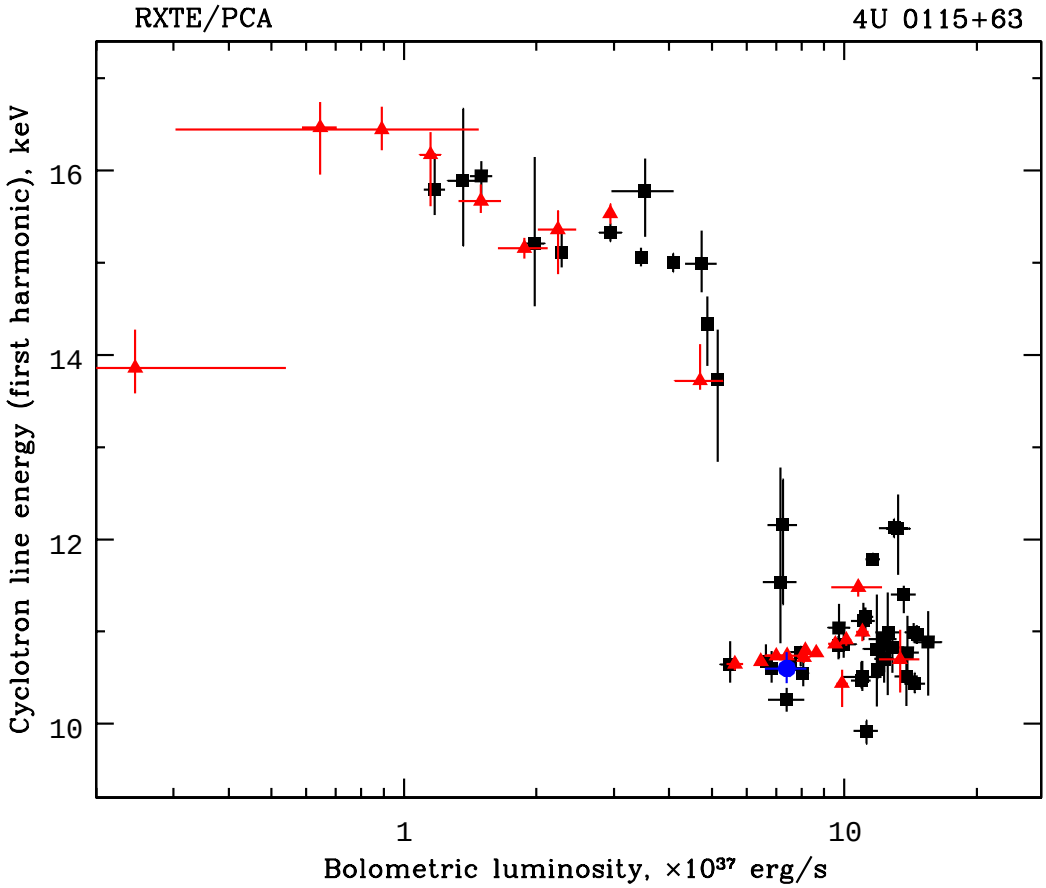

Fig. 12: Position of the fundamental harmonic of the cyclotron absorption line in the pulsar spectrum as a function of intrinsic luminosity. The squares, triangles, and circle indicate, respectively, the values during the 1999 outburst from RXTE data, during the 2004 outburst from RXTE data, and during the 2004 outburst from INTEGRAL data.

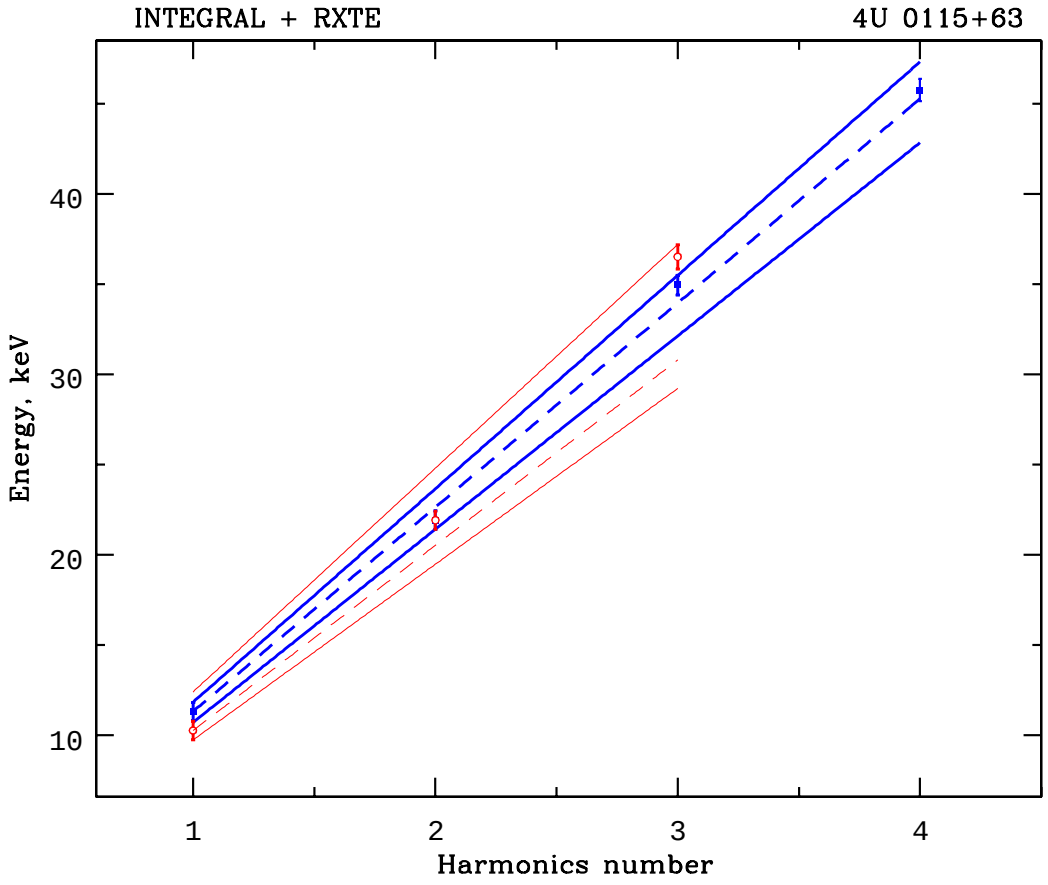

Fig. 13: Positions of the cyclotron line harmonics in the pulsar spectrum as a function of their numbers for two observations with different luminosities: 7.4×10^{37} erg s^{-1} from INTEGRAL data (filled squares and thick lines) and 11.0×10^{37} erg s^{-1} from RXTE data (open circles and thin lines). The dashed lines indicate the harmonic arrangement of harmonics; the solid lines indicate the maximum deviations from it.